Materials Today: Proceedings xxx (xxxx) xxx

Contents lists available at ScienceDirect

Materials Today: Proceedings

journal homepage: www.elsevier.com/locate/matpr

Freestanding 3D piezoelectric PVDF sensors via electroprinting

Kranthi Kumar Reddy Bannuru, Aby Raj Plamootil Mathai, Pablo Valdivia y Alvarado, Hong Yee Low *

Engineering Product Development, Singapore University of Technology and Design, 8 Somapah Road 487372, Singapore

ARTICLE INFO

Article history:
Available online xxxx

Keywords:
Electroprinting
PVDF solution
3D printing
Diw
Piezoelectric
Electrohydrodynamics

ABSTRACT

Polyvinylidene fluoride, PVDF is a soft piezoelectric material with potential applications in robotic sensors and actuators, wearable electronics, and energy harvesting. The sensitivity of piezoelectric PVDF is attributed primarily to the β-crystalline phase with oriented dipoles. 3D electroprinting process is a promising technique to achieve 3D PVDF-based piezoelectric devices because the combined mechanical stretching and electric field-assisted poling can improve the electroactive crystalline phases in PVDF. In this work, we show that the incorporation of an anti-solvent in the PVDF solution was instrumental in obtaining an optimum solution viscosity and solvent evaporation rate to achieve mechanically stable layer-by-layer printing. Two major process parameters further influencing the resolution of the printed structure were nozzle-to-collector distance and extrusion pressure. Freestanding 3D PVDF structures with an average individual layer height as small as 30 μm and continuous prints for multiple 3D designs have been achieved. FTIR and XRD spectra show an improvement in the electroactive β and γ phases in the electroprinted PVDF compared to the dominant α phase of PVDF powder. Furthermore, the 3D PVDF structures display sensitivity to various load profiles at varying frequencies with the piezoelectric voltage coefficient (g_{33}) range between 1.72E-4 and 4.08E-4 V.m/N.

Selection and peer-review under responsibility of the scientific committee of The International Conference on Additive Manufacturing for a Better World.

1. Introduction

Piezoelectric polymers are a subset of electroactive polymers (eEAP) that have been a subject of intense study as smart materials for applications in energy harvesting, health monitoring, wearable electronics, and soft robotics [1–10]. Polyvinylidene fluoride (PVDF) and its copolymers, namely poly(vinylidene fluoride-*co*-hexafluoropropylene) (PVDF-HFP) and poly(vinylidene fluoride-*co*-trifluoroethylene) (PVDF-TrFE) have been used in multifarious sensing applications in the form of spin-coated thin films, electrospun nanofiber mats as well as three-dimensional constructs [11–13]. Although piezoelectric properties of PVDF are lower than those of ceramics such as lead zirconate titanate (PZT), it is widely studied as an active layer for functional soft materials with electroactive properties due to the advantages of flexibility and low acoustic impedance besides being low cost, chemically inert and biocompatible [14]. PVDF is a semi-crystalline polymer with a repeating unit, $-CH_2CF_2$ having a dipole moment due to the high electronegativity of the fluorine atom. The molecular conformations and their packing control the orientation of dipoles where different phases of the crystal can be formed either as *trans*-(T) or *gauche* (G) linkage of a $-CH_2CF_2$ monomer unit [15]. PVDF exhibits five different polymorphs with distinct chain conformations identified as TTTT (all-*trans* planar zigzag) for the β phase, TGTG′ (*trans*-gauche–*trans*-gauche) for the α and δ phases, and T3GT3G′ for the γ and ε phases [16,17]. The α and ε phases have no electrical activity because the packing of their dipole moment is anti-parallel within the unit cell [18,19]. In the *β* phase, the dipole moment is the highest (8×10^{-30}C.m) [20] due to the alignment of all dipole chains in a single direction in an all-*trans* (TTTT) configuration that produces high spontaneous polarization in a unit cell. The improvement of β-phase fraction in PVDF has been a focus of research and is proven to improve piezo-, pyro-, and ferroelectric properties. [12,16,21].

The crystalline phases in PVDF are dependent on processing history, effects of solvents [22], mechanical stretching, and exposure to a polarizing external electrical field as they alter the ratio of the α and δ phases [12,13,19,23–25]. This possibility offers a clear advantage for using 3D electroprinting as an additive manufacturing (AM) technique to fabricate PVDF structures with enhanced design freedom in 3D piezoelectric structures. Moreover, 2D

* Corresponding author.
E-mail address: hongyee_low@sutd.edu.sg (H. Yee Low).

https://doi.org/10.1016/j.matpr.2022.09.364

Selection and peer-review under responsibility of the scientific committee of The International Conference on Additive Manufacturing for a Better World.

piezoelectric devices based on polymeric fibers or films do not capture the strain accumulation in the normal direction, and it can lead to reduced sensitivity of the piezoelectric response [46]. AM processes were previously reported to create 3D piezoelectric structures (Table 1). Among these AM processes, ink-jet printing, electrospinning (far-field and near-field), and 3D electrohydrodynamic jet (e-jet) printing rely on the principles of electrohydrodynamics, where the electric field drives the printed liquid. Exposure to an electric field causes the mobile ions in a polarizable fluid to accumulate at the liquid surface, potentially influencing the electrical properties of the printed material. In comparison to techniques like fused deposition modeling and melt electrowriting, polymer solutions in electroprinting present an advantage of achieving homogeneous blends for various polymer/nanomaterial combinations due to the presence of a solvent. Polymer solution-based processes are especially appealing for PVDF compared to melt-writing and fused filament fabrication due to the high melting points (~170 °C) and high melt viscosity.

However, direct writing of solvent-based inks is mostly limited to 2D or quasi-3D structures with limited resolution control. For instance, a common issue in direct writing of 3-D structure is the gradual solvent evaporation from freshly dispensed ink, resulting in the merging of printed adjacent layers and drooping of the top layer on the bottom layers. The rheological properties of the polymer solution must be optimized to obtain self-supporting multiple-layered structures without collapsing into each other during solvent evaporation. Here, we report a study on the effects of PVDF rheological properties and electroprinting process parameters in controlling the resolution of 3D printed PVDF structures. X-ray diffraction (XRD) and Fourier transform infrared (FTIR) spectroscopy were employed to investigate the effects of electroprinting on the crystalline phases of PVDF. Finally, the piezoelectric performance measurement tests were designed to measure the output voltage profile for various cyclical loads at varying frequencies.

2. Results and discussion

First, we established the solution parameters based on the solubility of PVDF, solvent evaporation rate, dynamic viscosity, and shear thinning behavior of polymer solution. PVDF is soluble in a variety of organic solvents such as Dimethylformamide (DMF), *N*-methyl pyrrolidine (NMP), dimethylsulfoxide (DMSO), and dimethylacetamide (DMAc) [29]. Among these solvents, we choose DMAc as it has a smaller distance (R_a) between Hansen parameters in Hansen space (R_a = 0.7) [30], and it has been suggested to be a more potent solvent for PVDF compared to others [31]. Acetone, a weak solvent for PVDF, evaporates faster than DMAc during the printing process. The rapid drying of the solution, which quickly converts the low viscosity solution to a near solvent-free solid, is essential to achieve mechanical support for the subsequent layer deposited on it without collapsing/spreading. However, higher concentrations of PVDF (>25 wt%) and a high percentage of acetone (>50 wt%) in the solvent mixture with DMAc led to a gel-like consistency. The rapid acetone evaporation resulted in nozzle clogs and a discontinuous fluid flow. An optimum solid content at 20–25 wt% PVDF and solvent concentration for acetone at 50 wt% of total solvent (Dmac/acetone) was found to achieve a stable uniform solution, printable viscosity, continuity of extrusion from the nozzle without clogs, and retention of the printed structure.

The addition of acetone as an anti-solvent has a non-linear effect on the mixture's viscosity, as shown in Fig. 1a. Typical values for the apparent solution viscosity in direct ink writing are 0.1–1000 Pa.s (depending on the shear rate) [32]. We note that 25 wt % PVDF in Dmac/acetone (1:1 wt/wt) offers a good balance with a relatively high apparent viscosity of 35.6 Pa.s (at a shear rate of 0.1 /s) and a higher relative amount of volatile solvent component (50 wt% acetone in the solvent mixture). The formulated solution also displays shear-thinning behavior for easy extrusion through the syringes and nozzles and regaining higher viscosity when the shear rate is removed upon deposition on the collector (Fig. 1b). Thus, it renders the ability to construct self-supporting layers after extrusion to maintain the printed structures as the solvent continuously evaporates after deposition. Based on the electroprinting of 20 wt% and 25 wt% PVDF solutions in Dmac/acetone (1:1 wt/wt) using nozzles of different gauges (24G to 30G), we used a 27G nozzle (D_n = 0.2 mm) in subsequent experiments to avoid both higher pressure of extrusion ($\Delta P > 0.6$ MPa) and frequent nozzle clogs.

The solution electroprinting process can be approximated to the theoretical model reported by Lei et al. to predict the feature size in electrohydrodynamic jet printing [33]. According to the Poiseuille-type flow, the jetting volume flow rate (Q) can be written as $Q = \frac{\pi D_n^4}{128 \mu L_n}\left(\Delta P + \frac{1}{2}\varepsilon_0 E^2 - \frac{2\gamma}{D_n}\right)$ where μ is the viscosity of the printing material, D_n and L_n are the nozzle inner diameter and length, respectively, ΔP is the extrusion pressure, ε_0 is the permittivity of a vacuum, E is the magnitude of the external electric field, and γ is the surface tension of the air–liquid interface. The air pressure (ΔP) and electric stress ($\frac{1}{2}\varepsilon_0 E^2$) must overcome the capillary pressure ($2\gamma/D_n$) to drive the flow of fluid through the thin nozzle. The calculated values for capillary pressure ($\gamma = 33.4 \pm 2.4$ mN/m measured by pendant drop using goniometer) and electric stress for different nozzle diameters and applied voltage are significantly lower compared to ΔP and thus have minimal effect on Q. Since the distance between nozzle and grounded substrate changes continuously during printing, the electric field experienced by the material is also changing. Thus, electric field strength, EFS = U/H, was maintained constant throughout the printing process by adjusting the voltage according to the distance between the nozzle and the collector (H) using the following formula.; $H = h_0 + (n-1)\Delta z$, where U is the voltage potential, h_0 is the initial distance between nozzle and collector, n is layer number, and Δz is the z-step increment in nozzle height per layer.

The printed layer width (x-y) of 100–200 μm and average layer height (z) of 30–45 μm were attained with varying parameters for extrusion pressure, voltage, and z-step when the nozzle-collector distance (h_0) is 0.2 mm (Fig. 2). Moreover, the nozzle's velocity and voltage were limited at smaller h_0 due to the proximity of the nozzle to the printed structure. The operating range of param-

Table 1
Reported additive manufacturing techniques for the fabrication of 3D piezoelectric structures using polymers and their composites in recent studies.

Method	Melt electrowriting [26]	Fused deposition model printing + thermal poling [27]	Projection stereolithography [28]	One-step 3D Print + poling [11]
Material	pvdf powder	pvdf/ $BaTiO_3$ (film-> filament)	f-PZT + photosensitive resin	pvdf/$BaTiO_3$/DMF/ acetone
Feature size	Fibre Ø: 17–55 μm	–	~ 20 μm (x-y), 15 μm (z)	~ 0.6 mm (x-y)
Piezosensitivity	$d_{33} \approx 19$ pm/V (PFM)	$d_{31} = 2.9\text{x}10^{-3}$ (unpoled), $21\text{x}10^{-3}$ pC/N (poled)	$g_{33} \approx 0.75$ V.m/N (max)	Max. specific charge output ~ 2pC/mm^2
Application	–	–	Designed anisotropy and force directional sensing	Gait monitoring sensor

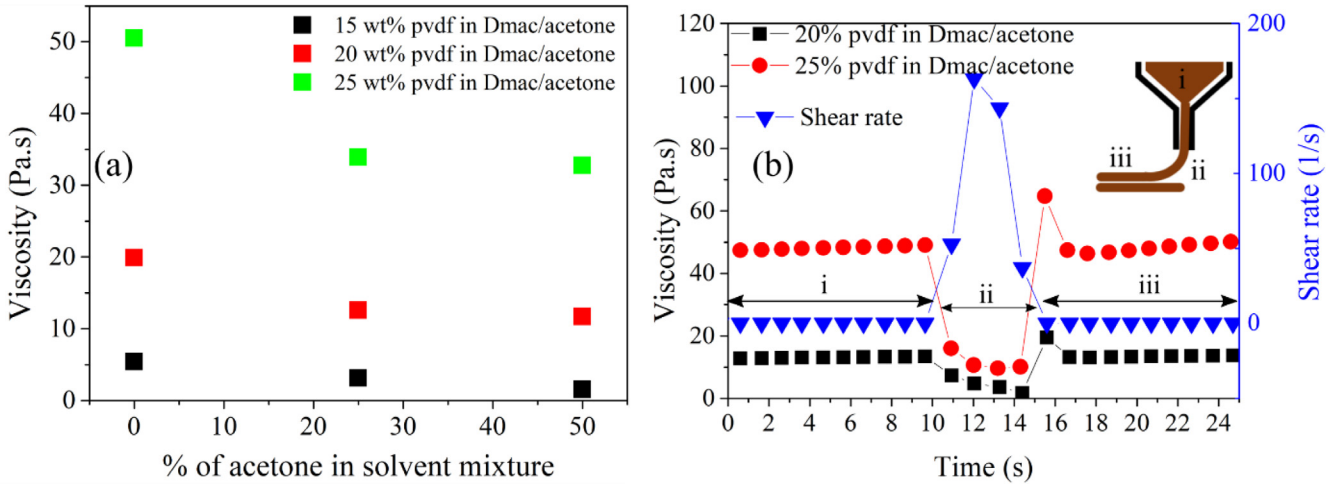

Fig. 1. Rheological characterization of PVDF solutions. (a) Viscosity measurements of varying concentrations of PVDF and the relative ratio of acetone in the solvent mixture. The presence of acetone as an anti-solvent decreases the viscosity. It promotes solvent evaporation after extrusion (b) Viscosity profile for PVDF solutions in response to quick changes in shear rates. The regions i, ii, iii correspond to the shear rate experienced by the fluid in the barrel, extrusion through a nozzle onto the substrate, and after deposition, respectively.

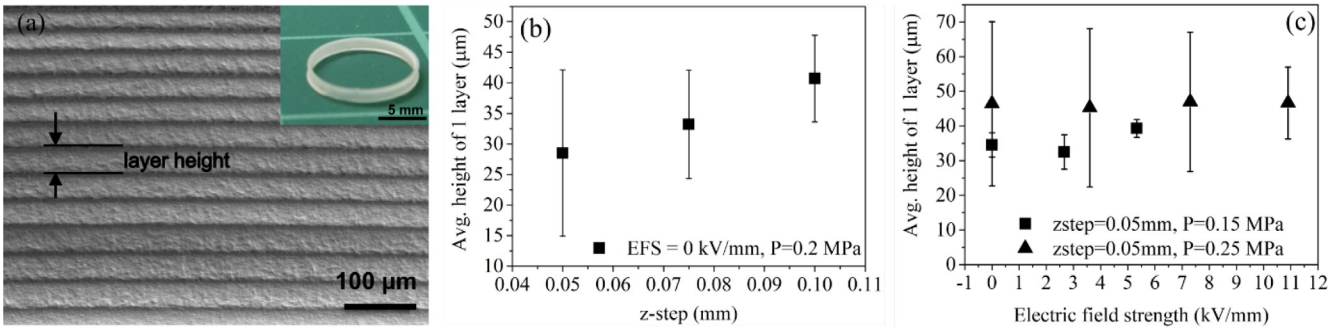

Fig. 2. Effect of electroprinting parameters on the average individual layer height (a) SEM image of the wall surface of a portion cut from a 3D cylindrical wall (Inset: photograph of printed structure consisting of 20 layers ((D_n = 0.2 mm; V_{nozzle} = 2 mm/s; h_0 = 0.2 mm; U = 0 kV). (b) Effect of the value of z-step increment on the layer height for ΔP = 0.2 MPa (c) Effect of varying electric field strength on the layer height for Δz = 0.05 mm and ΔP = 0.15, 0.25 MPa.

eters for electroprinting of 20 wt% and 25 wt% PVDF solutions at h_0 = 0.2 mm are listed in Table 2. When h_0 is increased, the jet-stretching and solvent evaporation rate is enhanced to produce a finer layer on the collector. The electroprinting method has accommodated h_0 up to 3 mm (with a corresponding U up to 3 kV) for 20 wt% PVDF solution to produce a single layer print with a width ~ 1 µm, as seen in Fig. 3a. The printing time is also reduced, especially for straight-line paths without sharp turns, as electroprinting has achieved 75 layered prints with the velocity of the nozzle up to 40 mm/s without interruption. Despite achieving ~ 1 µm line width for single layer prints with the above conditions, we observed that the overall dry 3D structure has a base width of ~ 650 µm (Fig. 3b). The thin jet that undergoes stretching tends to be unstable and deviate from the print path to be deposited on the Al surface instead of the previously deposited PVDF layer, thus leading to a broad base of the 3D structure.

SEM images in Fig. 4 show the morphology of electroprinted 3D PVDF freestanding structures in two different designs – a closed rectangular wall and a lattice structure, with the outer interface between the layers and its cross-section area. The outer surface of the structure appears porous with granular particles, which can be explained by vapor-induced phase separation [34] as the structures are printed at ambient temperature and humidity. The difference in microstructures of designs could be attributed to differences in the time available for the solvent evaporation of a printed layer before the next layer is printed on it. Also, the overlap of the adjacent layers in the presence of an unevaporated solvent can be seen in Fig. 4b, where less time is available for solvent evaporation between adjacent layers owing to print design. Furthermore, the intersection point of the lattice structure disrupted the continuous printing of a higher number of layers due to the excess solution at the intersection, causing a bulge colliding with the nozzle nearby.

XRD characterization in Fig. 5a confirms that the PVDF powder is primarily composed of the α phase, as indicated by two strong diffraction peaks at 18.0° (020) and 19.6° (110), a medium peak at 26.6° (021) and weak peaks at 32.7 (130), 35.5 (200), 38.5 (002) corresponding to monoclinic α crystal phase [35]. For

Table 2
The operating range of parameters for electroprinting 20 wt% and 25 wt% PVDF solutions. (D_n = 0.2 mm, h_0 = 0.2 mm).

Print Design	Substrate	EFS (kV/mm)	No. of layers	ΔP (MPa)	V (mm/s)	Δz (mm)
Non-intersecting	Aluminium	0–1	1–20	0.1–0.35	1–8	0.02–0.07
Non-intersecting	Glass coverslip	0–11	1–20	0.1–0.35	1–8	0.02–0.07
Intersecting	Aluminium	0–0.8	1–12	0.1–0.3	1–6	0.02–0.05

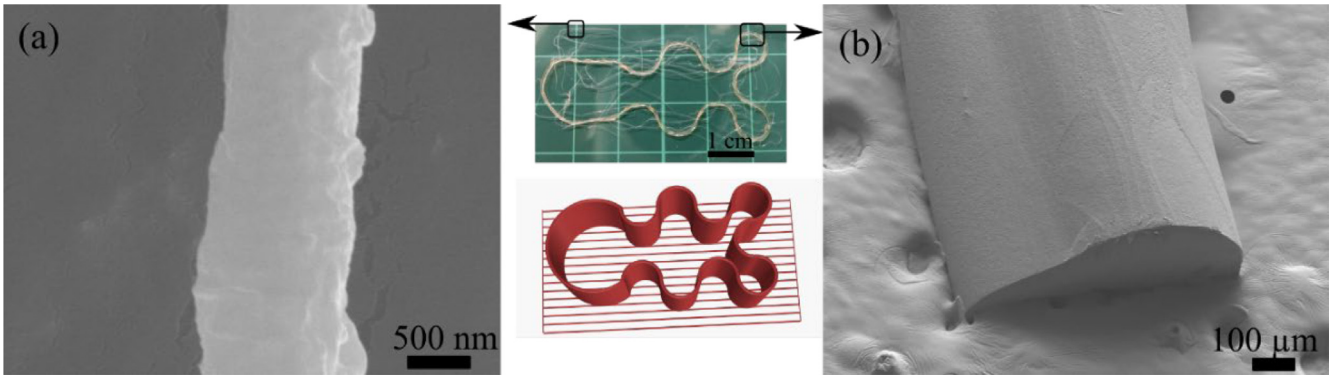

Fig. 3. PVDF structures are printed at a nozzle-collector distance (h_0) of 3 mm. The digital photograph and design consist of a single layer of PVDF as the base (seen as attached random fibers) and the serpent design for the 3D structure of 75 layers. (a) SEM image of a single fiber from the base layer. (b) Tilted view SEM image of 3D PVDF structure after drying under vacuum. Parameters of electroprinting: 20 wt% PVDF solution, D_n = 0.15 mm, U = 3 kV, V_{nozzle} = 40 mm/s, P = 0.1 MPa, z-step = 0.02 mm, Al substrate).

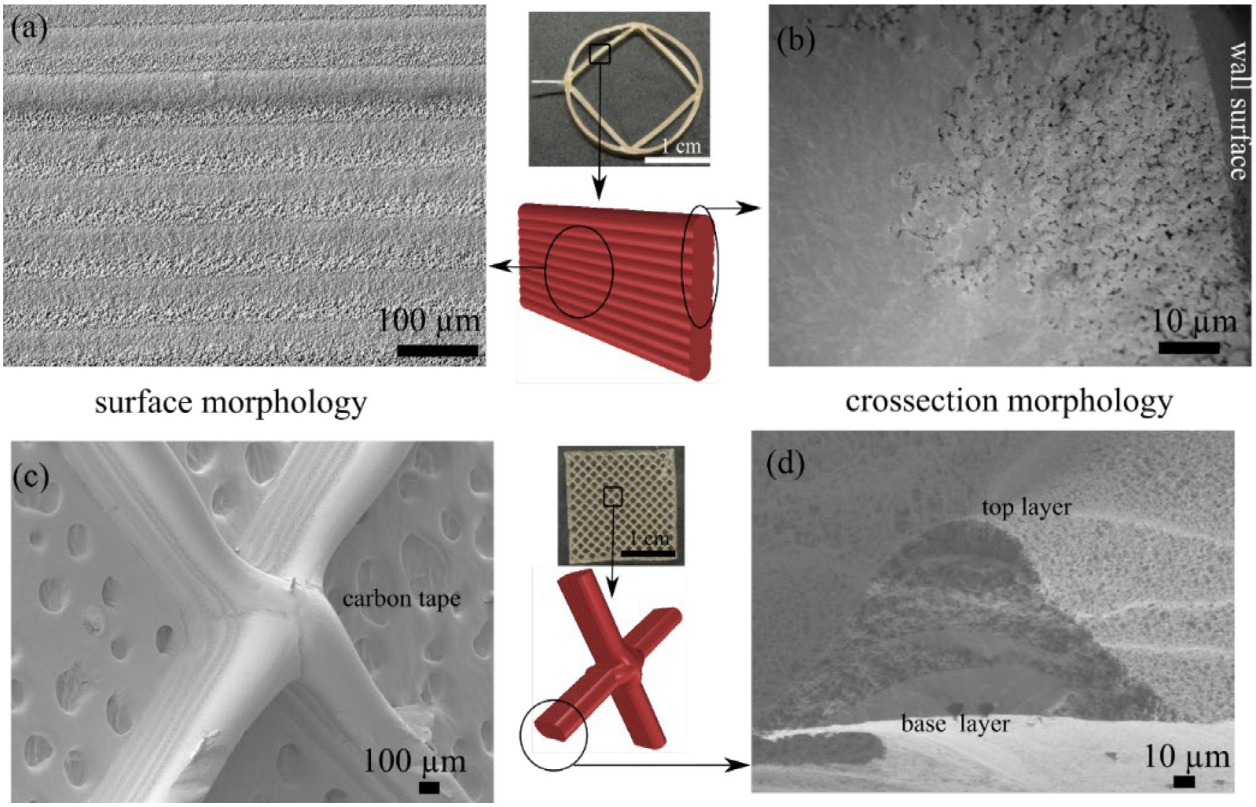

Fig. 4. SEM images of structures fabricated by electroprinting on Al substrate and the print design's graphical representation (V_{nozzle} = 4 mm/s; h_0 = 0.2 mm). (a,b) rectangular wall structure depicting the outer surface of the layers and the crossection area, respectively. (c, d) lattice structure with intersecting region depicting the outer surface of the layers and the crossection area, respectively.

solution-cast PVDF film and electroprinted PVDF structures, the peaks corresponding to the α phase have diminished, and new peaks corresponding to electroactive β and γ phases have appeared. Previous works using PVDF films and electrospun fibers have reported XRD data with peaks around 20° corresponding to α, β, and γ phases and peaks around 18° corresponding to α and γ phases [11,12,16]. A study by Cai et al. on critical analysis of the phases of PVDF using FTIR and XRD identifies the presence of strong peaks at 18.4° (020), 20.0° (110), and weak peaks at 26.6° (021) and 35.9° (200) with α phase; the presence of a strong peak at 20.6° (110)/(200) and weak peak at 36.3° with β phase; and strong peak at 20.3° (110)/(101) and medium peaks at 18.5° (020) and 39.0° (211) with γ phase of PVDF. In another detailed study by Martins et al., some peaks corresponding to α and γ phases of PVDF were attributed differently [16]. The intense broad peak in the range of 20.2° to 20.6° has been attributed to either β-phase or γ-phases in combination with the absence or presence respectively of the peak at 18.5°. XRD spectra are helpful to distinguish the exclusive β-phase when observed as the only broad and intense peak around 20.2° in the absence of other peaks around 18° [16].

As shown in Fig. 5a, 3D electroprinted PVDF shows a strong, broad peak at 20.2° (β or γ) in addition to a medium peak at 18.6° (γ) and weak peaks at 36.3° (β) and 39.3° (γ) with almost none of the peaks corresponding to α phase in PVDF powder. To further confirm the improvement in the relative quantity of β

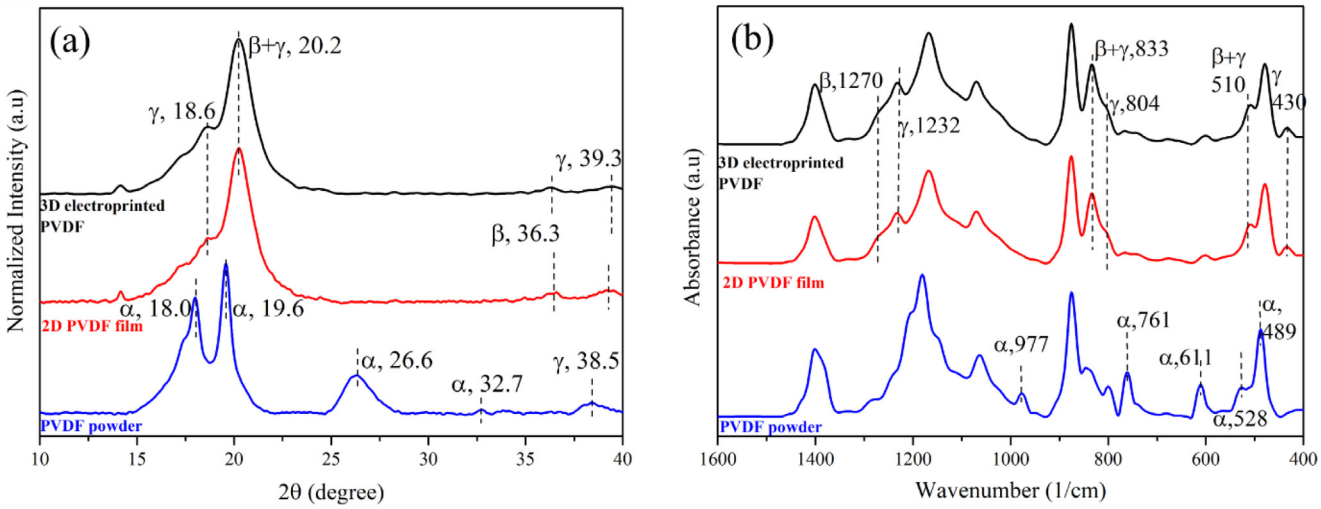

Fig. 5. (a) X-ray diffractogram and (b) FTIR spectra of commercial PVDF powder, solution cast PVDF film, and electroprinted PVDF structures, with peak labels of the corresponding phases.

and γ phases in the printed structures, we compare the FTIR spectral bands for PVDF powder, solution cast PVDF film, and 3D PVDF samples in Fig. 5b. The absorption bands at 489 cm^{-1}, 611 cm^{-1}, 761 cm^{-1}, 977 cm^{-1} corresponding to the α phase in PVDF powder [16,35] are absent in the PVDF film and 3D samples. Instead, the characteristic bands for the β phase at 1270 cm^{-1} and the γ phase at 1232 cm^{-1} confirm the presence of the polar phases (β and γ) in the printed structure sample. The XRD and FTIR analysis show that the crystalline phases in the electroprinted PVDF are comparable to the solvent cast PVDF film and an improvement over the raw powder.

To evaluate the piezoelectric sensitivity of the electroprinting of 3D PVDF structures, we employed an electroforce system to apply a controlled load of 20 N peak-peak on the 3D perpendicular lattice construct shown in Fig. 4c (with a thickness of 210 μm and an active area of 55 mm^2) attached with Cu tape on both faces as electrodes. The input to the sensor consists of different load profiles (sine, square, triangular) at varying frequencies (5 Hz,10 Hz, 20 Hz), as seen in Fig. 6a. We observed a voltage response from the PVDF sensor in Fig. 6 (c, d, e) corresponding to the change in frequency for each load profile input indicating the piezoelectric functionality of the sensor over a broad spectrum of input loads. Moreover, the voltage generated is consistent over many cycles without loss in the voltage response. The piezoelectric voltage constant for each load condition was calculated using the equation: $V_{out} = \frac{|g_{33}| \times t \times F}{A}$ Where g_{33} is the piezoelectric voltage constant in

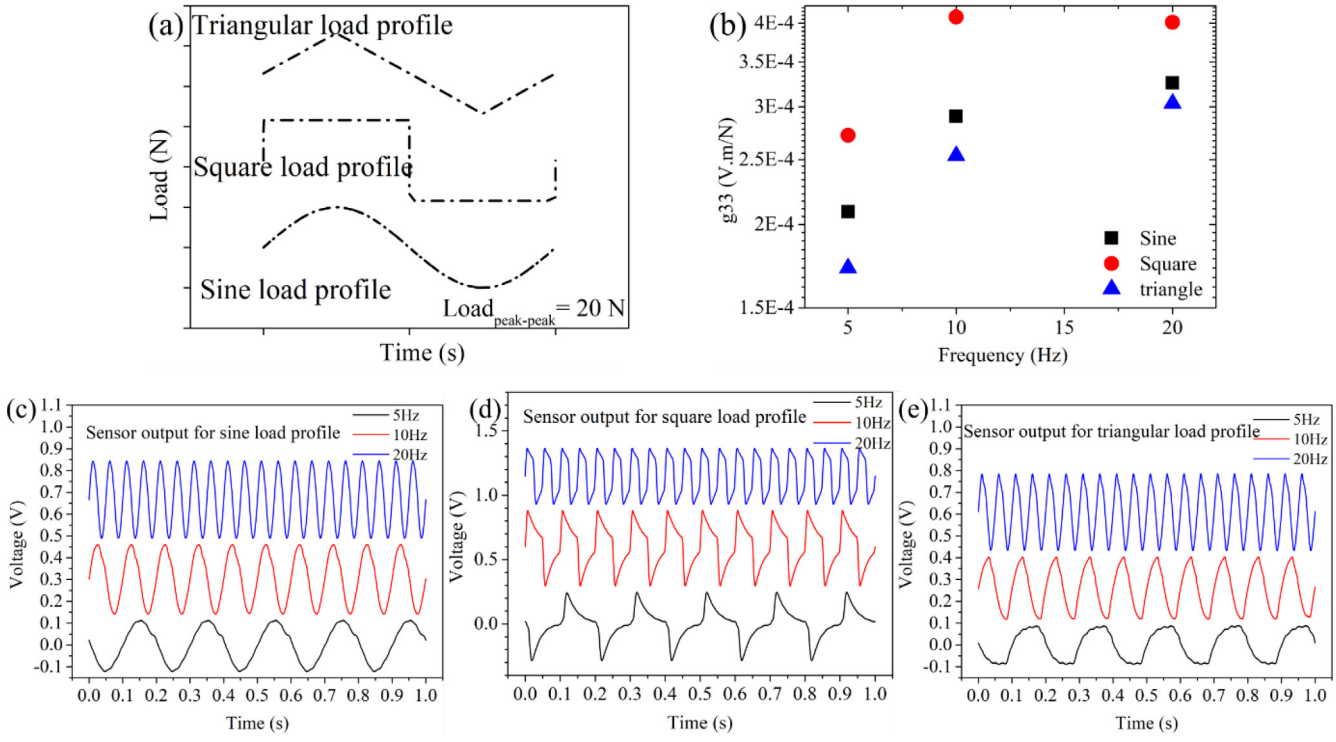

Fig. 6. Piezoelectric sensitivity of electroprinted 3D PVDF structures. (a) Load profiles are applied as force input to the sensor at frequencies of 5 Hz, 10 Hz, 20 Hz with an amplitude of 10 N ($Load_{peak-peak}$ = 20 N). (b, c, d) Sensor output voltage response for sine, square, triangular load profiles respectively at frequencies of 5 Hz (black), 10 Hz (red), 20 Hz (blue). e) Calculated values of piezoelectric voltage constant (g_{33}) based on the voltage generated by the sensor and the input load for different frequencies and load profiles. (For interpretation of the references to colour in this figure legend, the reader is referred to the web version of this article.)

the z-direction, t is the overall height of the structure in the z-direction of the PVDF structure, F is the load applied, and A is the active PVDF sensor area [43], [44]. The longitudinal piezoelectric voltage coefficient (g_{33}) values for the electroprinted 3D PVDF sensor with a 20 N peak-peak cyclical load input are calculated to be in the range of 1.72E-4 to 4.09E-4 V.m/N (Fig. 6b). It is observed to change with the frequency and type of load. The change in load over time is gradual for sine, triangular profiles, whereas the change is sudden for the square profile.

3. Conclusion

3D Electroprinting presents an emerging AM process to fabricate freestanding 3D piezoelectric structures from PVDF solutions. Polymer solutions of 20 wt% and 25 wt% PVDF in Dmac/acetone (1:1 wt) were chosen for electroprinting based on the viscosity, shear-thinning behavior, and the ability to form self-supporting structure after extrusion. Extrusion pressure has a notable impact on the volume flow rate of solution from the nozzle and thus determines the print feature width and height notably compared to z-step or electric field strength. The electric field strength of 0.8–1 kV/mm between nozzle and collector is found to be ideal for a straight focused jet and to avoid the breakdown of air during printing. The nozzle-collector distance up to 3 mm yielded continuous prints with nozzle-velocity 40 mm/s and up to 75 layers. Still, the final structure showed a base width of $\sim$ 650 μm despite depositing a $\sim$ 1 μm wide single layer (measured after drying of solvent). The relative quantity of the electroactive β and γ phases of PVDF were dominant in the electroprinted samples compared to the raw powder. The sensors fabricated from electrprinted 3D PVDF structures were sensitive to different load profiles at varying frequencies (5 Hz,10 Hz, 20 Hz) and showed output voltage profiles to distinguish the type of load. The piezoelectric voltage coefficient (g_{33}) for the loads ranges between 1.72E and 4 and 4.08E-4 V.m/N. Thus, solution-phase processing of polymers via electroprinting offers a facile route toward 3D functional structures, especially for polymers with a high melting point and melt viscosity.

4. Materials and methods

PVDF (Mw $\sim$ 534 000), dimethylacetamide (DMAc, 99.5 %), were purchased from Sigma-Aldrich, and acetone (99.9 %) from Elite advanced materials. PVDF powder is mixed with a 1:1 Dmac/acetone and stirred at 80 °C for 4 h under ambient conditions and continued to stir at room temperature for 1 h before printing.

PVDF solutions were deposited via electroprinting using a modified direct ink writing (DIW) printer consisting of a 3D printing robot, a dispenser (IMAGE MASTER 350PC Smart SMΩX, Musashi Engineering Inc., Japan), and an external high voltage source. The liquid dispenser was equipped with a syringe loaded with PVDF solution, and it was attached to a precise pneumatic controller (ML-5000XII, Musashi Engineering Inc., Japan). A glass slide attached with aluminum tape on top is placed on the heat bed as the conductive print substrate. A high voltage DC power supply (E-star Group technology Co. ltd., China) was used to generate an electric field between the nozzle and the collector surface. The positive terminal of the high voltage supply is connected to the nozzle and the ground terminal to the Al foil using alligator clips. MuCAD V software (Musashi Engineering Inc., Japan) and Rhino 6 software were used to generate the 3D designs for electroprinting. PVDF polymer solution was loaded into cylindrical dispensing barrels attached with blunt needles for printing. PVDF solution was extruded through the attached nozzle to form a filament deposited onto the Al collector surface. The extrusion pressure, dispensing head velocity (in ×, y, z directions), dispensing head acceleration, and deceleration times were determined based on the geometry of the print and viscosity of the ink.

Scanning Electron Microscope (SEM) images were taken with a JSM-7600F Field Emission SEM (JEOL, Japan). Before imaging, the samples were sputtered with gold in a vacuum for 60 s with a current of 30 mA. FTIR spectra were obtained in attenuated total reflection (ATR) mode on a PerkinElmer Frontier FTIR spectrometer with a germanium ATR top plate and 1.3 mm crystal diameter. Measurements consisted of 32 scans at 4 cm^{-1} resolution. The PVDF crystalline phases were characterized by X-ray diffraction (XRD, Bruker D8Advance) using the Cu Kα (λ = 0.154 nm) radiation lines with the accelerating voltage of 40 kV. The viscosity tests were conducted on a Discovery Hybrid Rheometer (DHR2, TA instruments Inc., UK) with an aluminum parallel plate geometry (20 mm in diameter) at ambient conditions. The plate gap was set as 1000 μm.

The piezoelectric response of the PVDF structures fabricated by electroprinting was measured by subjecting them to dynamical compression pressure on the Electroforce 3200 test system (TA instruments). The applied load profile consisted of sine, square, triangular waves with a load of 10 N and varied frequencies of 5 Hz, 10 Hz, 20 Hz. Cu tape with soldered connections was used as the electrode on both sides of PVDF film and the printed PVDF lattice structures. The PVDF sensor was held between the top and bottom plates of the electroforce system at an initial load of 0.1 N before running the test with the load profile. The signal from the PVDF sensor was fed into a piezo lab pre-amplifier (Measurement Specialities, USA) in voltage mode with a gain of 20 dB, and a frequency bandpass filter (0.1 Hz to 100 Hz, filter gain −3dB) and the output was acquired on an oscilloscope.

CRediT authorship contribution statement

Kranthi Kumar Reddy Bannuru: Conceptualization, Methodology, Writing – original draft, Writing – review & editing, Data curation, Investigation, Visualization. **Aby Raj Plamootil Mathai:** Methodology, Writing – review & editing. **Pablo Valdivia y Alvarado:** Supervision, Writing – review & editing. **Hong Yee Low:** Conceptualization, Methodology, Writing – review & editing, Supervision.

Data availability

Data will be made available on request.

Declaration of Competing Interest

The authors declare that they have no known competing financial interests or personal relationships that could have appeared to influence the work reported in this paper.

Acknowledgements

KKRB is grateful for the president's graduate fellowship from Singapore University of Technology and Design.

References

[1] S. Park, Y. Kim, H. Jung, J.-Y.-Y. Park, N. Lee, Y. Seo, Energy harvesting efficiency of piezoelectric polymer film with graphene and metal electrodes, Sci. Rep. 7 (1) (Dec. 2017) 1–8.

[2] S. Sukumaran, S. Chatbouri, D. Rouxel, E. Tisserand, F. Thiebaud, T. Ben Zineb, Recent advances in flexible PVDF based piezoelectric polymer devices for energy harvesting applications, J. Intell. Mater. Syst. Struct., Apr. 32 (7) (2021) 746–780.

[3] M. Pan, C. Yuan, X. Liang, J. Zou, Y. Zhang, and C. Bowen, "Triboelectric and Piezoelectric Nanogenerators for Future Soft Robots and Machines," *iScience*, vol. 23, no. 11, p. 101682, Nov. 2020.
[4] M. Haq, Application of piezo transducers in biomedical science for health monitoring and energy harvesting problems, Mater. Res. Express 6 (2) (Feb. 2019) 22002.
[5] W.H. Duan, Q. Wang, S.T. Quek, Applications of piezoelectric materials in structural health monitoring and repair: Selected research examples, Materials (Basel) 3 (12) (2010) 5169–5194.
[6] X. Wang et al., Bionic single-electrode electronic skin unit based on piezoelectric nanogenerator, ACS Nano 12 (8) (Aug. 2018) 8588–8596.
[7] Z.Z. Li, Q. Zheng, Z.L. Wang, Z.Z. Li, Nanogenerator-based self-powered sensors for wearable and implantable electronics, Research 2020 (Mar. 2020) 1–25.
[8] Y. Zhou, J. He, H. Wang, K. Qi, N. Nan, X. You, W. Shao, L. Wang, B. Ding, S. Cui, Highly sensitive, self-powered and wearable electronic skin based on pressure-sensitive nanofiber woven fabric sensor, Sci. Rep. 7 (1) (2017).
[9] W. Liu, A. Menciassi, S. Scapellato, P. Dario, Y. Chen, PVDF-based biomimetic sensor for application in crawling soft-body mini-robots, in: In *IEEE International Conference on Intelligent Robots and Systems*, 2006, pp. 1960–1965.
[10] F. Wang, X. Zhao, and J. Li, "PVDF energy-harvesting devices: Film preparation, electric poling, energy-harvesting efficiency," in *Annual Report - Conference on Electrical Insulation and Dielectric Phenomena, CEIDP*, 2015, vol. 2015-Decem, pp. 80–83.
[11] S. Bodkhe, P.S.M. Rajesh, F.P. Gosselin, D. Therriault, Simultaneous 3D Printing and Poling of PVDF and Its Nanocomposites, ACS Appl. Energy Mater. 1 (6) (Jun. 2018) 2474–2482.
[12] C. Chen et al., 3D printing of electroactive PVDF thin films with high β-phase content, Smart Mater. Struct. 28 (6) (2019) 65017.
[13] C. Ribeiro, C.M. Costa, D.M. Correia, J. Nunes-Pereira, J. Oliveira, P. Martins, R. Gonçalves, V.F. Cardoso, S. Lanceros-Méndez, Electroactive poly(vinylidene fluoride)-based structures for advanced applications, Nat. Protoc. 13 (4) (2018) 681–704.
[14] S. Bauer, F. Bauer, N. Murayama, and H. Obara, "Piezoelectric Polymers and Their Applications," in *Springer Series in Materials Science*, vol. 114, Berlin, Heidelberg: Springer Berlin Heidelberg, 2008, pp. 157–177.
[15] T. Furukawa, Ferroelectric properties of vinylidene fluoride copolymers, Phase Transitions 18 (3–4) (Aug. 1989) 143–211.
[16] P. Martins, A.C. Lopes, S. Lanceros-Mendez, Electroactive phases of poly (vinylidene fluoride): determination, processing and applications, Prog. Polym. Sci. 39 (4) (2014) 683–706.
[17] A.J. Lovinger, Poly(Vinylidene Fluoride), in: D.C. Bassett (Ed.), Developments in Crystalline Polymers—1, Springer Netherlands, Dordrecht, 1982, pp. 195–273.
[18] B. Ameduri, From vinylidene fluoride (VDF) to the applications of VDF-Containing polymers and copolymers: recent developments and future trends, Chem. Rev. 109 (12) (Dec. 2009) 6632–6686.
[19] S. M. Damaraju, S. Wu, M. Jaffe, and T. L. Arinzeh, "Structural changes in PVDF fibers due to electrospinning and its effect on biological function," *Biomed. Mater.*, vol. 8, no. 4, 2013.
[20] A.J. Lovinger, Conformational defects and associated molecular motions in crystalline poly(vinylidene fluoride), J. Appl. Phys. 52 (10) (Oct. 1981) 5934–5938.
[21] P. Martins et al., Local variation of the dielectric properties of poly(vinylidene fluoride) during the α- to β-phase transformation, Phys. Lett. Sect. A Gen. At. Solid State Phys. 373 (2) (2009) 177–180.
[22] T. Nishiyama, T. Sumihara, E. Sato, H. Horibe, Effect of solvents on the crystal formation of poly (vinylidene fluoride) film prepared by a spin-coating process, Polym. J. 49 (3) (2017) 319–325.
[23] J. Zheng, A. He, J. Li, C.C. Han, Polymorphism control of poly(vinylidene fluoride) through electrospinning, Macromol. Rapid Commun. 28 (22) (2007) 2159–2162.
[24] X. Wang, F. Sun, G. Yin, Y. Wang, B. Liu, and M. Dong, "Tactile-sensing based on flexible PVDF nanofibers via electrospinning: A review," *Sensors (Switzerland)*, vol. 18, no. 2. 2018.
[25] P.K. Szewczyk et al., Enhanced piezoelectricity of electrospun polyvinylidene fluoride fibers for energy harvesting, ACS Appl. Mater. Interfaces 12 (11) (2020) 13575–13583.
[26] S. Florczak et al., Melt electrowriting of electroactive poly(vinylidene difluoride) fibers, Polym. Int. 68 (4) (Apr. 2019) 735–745.
[27] H. Kim, T. Fernando, M. Li, Y. Lin, T.-L.-B. Tseng, Fabrication and characterization of 3D printed $BaTiO_3$ /PVDF nanocomposites, J. Compos. Mater. 52 (2) (Jan. 2018) 197–206.
[28] H. Cui et al., Three-dimensional printing of piezoelectric materials with designed anisotropy and directional response, Nat. Mater. 18 (3) (Mar. 2019) 234–241.
[29] A. Bottino, G. Capannelli, S. Munari, A. Turturro, Solubility parameters of poly (vinylidene fluoride), J. Polym. Sci. Part B Polym. Phys. 26 (4) (1988) 785–794.
[30] Prof Steven Abbott, "Hansen Solubility Parameters." [Online]. Available: https://www.hansen-solubility.com/HSP-science/solvent-blends.php.
[31] M.L. Yeow, Y.T. Liu, K. Li, Isothermal phase diagrams and phase-inversion behavior of poly(vinylidene fluoride)/solvents/additives/water systems, J. Appl. Polym. Sci. 90 (8) (2003) 2150–2155.
[32] J.A. Lewis, Direct ink writing of 3D functional materials, Adv. Funct. Mater. 16 (17) (Nov. 2006) 2193–2204.
[33] L. Qian, H. Lan, G. Zhang, A theoretical model for predicting the feature size printed by electrohydrodynamic jet printing, Appl. Phys. Lett. 112 (20) (May 2018) 203505.
[34] M. Li et al., Controlling the microstructure of poly(vinylidene-fluoride) (PVDF) thin films for microelectronics, J. Mater. Chem. C 1 (46) (Dec. 2013) 7695–7702.
[35] X. Cai, T. Lei, D. Sun, L. Lin, A critical analysis of the α, β and γ phases in poly (vinylidene fluoride) using FTIR, RSC Adv. 7 (25) (Mar. 2017) 15382–15389.